Numerical dynamic analysis of reciprocating compressor mechanism. Parametric studies for optimization purposes

A. Pont, J. López, J. Rigola, C.D. Pérez-Segarra

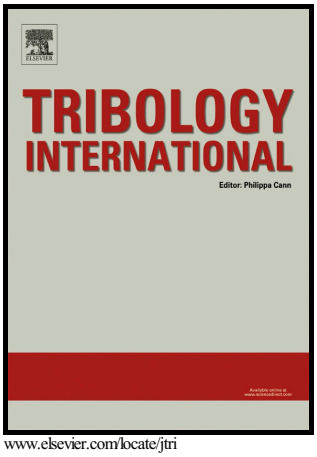

www.elsevier.com/locate/jtri

PII: S0301-679X(16)30190-6
DOI: http://dx.doi.org/10.1016/j.triboint.2016.06.019
Reference: JTRI4251

To appear in: *Tribiology International*

Received date: 15 March 2016
Revised date: 13 June 2016
Accepted date: 14 June 2016

Cite this article as: A. Pont, J. López, J. Rigola and C.D. Pérez-Segarra Numerical dynamic analysis of reciprocating compressor mechanism. Parametri studies for optimization purposes, *Tribiology Internationa* http://dx.doi.org/10.1016/j.triboint.2016.06.019

Numerical Dynamic Analysis of Reciprocating Compressor Mechanism. Parametric Studies for Optimization Purposes.

Pont, A.*, López, J.*, Rigola, J.*, Pérez-Segarra, C.D.*

Heat and Mass Transfer Technological Centre (CTTC), Universitat Politècnica de Catalunya - BarcelonaTech (UPC), ESEIAAT, Carrer Colom 11, 08222 Terrassa (Barcelona), Spain.

Abstract

A complete numerical dynamic analysis of reciprocating compressor mechanism is presented, coupling the instantaneous pressure in the compression chamber, the electric motor torque and the hydrodynamic reactions, which arise from the piston and crankshaft secondary movements. Additionally, non-constant crankshaft angular velocity and the piston and crankshaft misalignment torques have also been considered. Two sensitivity analyses have been carried out to prove that neither the inertial forces in the directions of the secondary movements, nor the oscillations of the angular velocity produce significant differences in the compressor behaviour. Finally, a set of parametric studies have been developed to evaluate the influence of geometrical parameters in the stability of the secondary movements, the friction power losses and the compressor consumption.

Keywords: Numerical analysis, Reciprocating, Lubrication, Journal

*Corresponding author
Email address: cttc@cttc.upc.edu (Pont, A.)

1. Introduction

The reciprocating compressors are widely used in the refrigeration world. During the last half century several experimental and numerical studies have been carried out to improve the performance and the entire lifetime of these devices. These studies are focused on the most basic mechanism, e.g. journal bearings to the most complex system, e.g. the compressor itself.

One of the most important parts of these compressors consists of the reciprocating mechanism coupled with instantaneous pressure in the compression chamber and the electric motor torque. The reciprocating mechanism is composed of the piston, the connecting-rod and the crankshaft. Each of these elements have a primary motion which is macroscopic, and a secondary motion which is microscopic. Only the secondary motion of the piston and the crankshaft is considered. Both secondary movements depend on the lubrication elements. In the piston case, the lubrication element is the cylinder-piston cavity, while the lubrication elements of the crankshaft are their journal bearings. Each of these components have been studied separately. They are well explored topics in the literature.

During the sixties, Campbell et al. [1] reviewed the numerical and experimental studies of the journal bearing behaviour under dynamic loads. The results presented in this review have been used in this work to validate the algorithm that calculates the crankshaft trajectories. Other researches were focused on this area, e.g. Booker, J.F. [2] and Jones, G.J. [3]. Booker created the mobility method which can easily predict the journal bearing behaviour under dynamic loads using low computational resources. Nonetheless, Biao, Yu [4] demonstrates in his research that the difference between the rigorous method and the mobility method can be higher than 70% in some cases. The Reynolds equation was used in all these studies to calculate the pressure field around the bearing. However, during the last decade some studies which use CFD techniques have appeared. One of them is Gertzos, K.P. [5]. This author uses a commercial software to simulate a 3-D CFD journal bearing lubricated by Newtonian or Bingham lubricants. These results have been used in this document to validate the aligned journal bearing eccentricity, and its load angle as function of the Sommerfeld number.

All these studies on journal bearings are necessary to understand the ring-less piston secondary motion since it works like a journal bearing. Thus, the Reynolds equation can also be used to calculate the pressure distribution around this kind of pistons. The ring-less technique is used to decrease the

friction losses of the compressors. However, two main problems appear when the piston rings are avoided. Firstly, the fluid leakage around the clearance is increased and it can affect the compressor performance. Secondly, the piston loses stability and it can slap the cylinder walls, producing a high increase of the wear. These two problems were studied by Li, D.F. et al. [6], for V8 gasoline engines. Li, D.F. studied the influence of the wrist-pin position to control the friction forces and the stability. His work was motivated for the visual studies carried out using transparent cylinders [7; 8]. These studies showed the importance of the thin layer of oil to delay the piston slaps. Later on Zhu, D. et al. [9; 10] developed some studies related to the engine mechanism and the piston secondary motion, as Li, D.F. This author considered piston surface waviness, roughness, piston skirt surface profile, bulk elastic deformation and thermal distortions. Afterwards, Prata, A.T. [11] studied the same phenomena in reciprocating compressors. Subsequent studies, e.g. Kim, T.-J. [12], developed new models able to calculate the piston secondary motion considering that the piston could protrude from the inside of cylinder bore due to the shortened length of the cylinder chamber. Both Prata and Kim studies supposed a crankshaft constant angular velocity. Rigola, J. [13; 14] analysed the piston leakage and its stability using a numerical pressure distribution in the pressure chamber and experimental data for the electric motor torque. This study took into consideration that the crankshaft angular velocity was not constant. Furthermore, the elastohydrodynamic lubrication (EHD) was implemented by Cho, J. [15] in the piston case. Cho, J. developed an algorithm coupling the lubrication equation with the finite element method to solve the structural deformation. Today the piston dynamics continues to be an active research topic. Some authors as Meng, X. et al. [16] have worked recently in a new model which couples the tribological performance of the piston skirt-liner system with the dynamics of the connecting rod, the crankshaft, the flywheel, and the piston. In the model, the piston secondary motion and the crankshaft angular acceleration of the crankshaft are both considered. However, this work does not consider the crankshaft secondary movement and how they are affected by the other compressor elements.

The journal bearings also affect the crankshaft stability. Several studies can be found in the literature which study the rotor stability limited for a system of two bearings. One of the most recent and complete work has been carried out by Liu, H. [17]. This author studied the rotor-bearing system, coupling the CFD and fluid-structure interaction (FSI) techniques. His study

was focused on different materials and showed that the rotor trajectories were not significantly affected by the structural deformation of the rotor-bearing system made of steel.

Despite there are several studies focused on the different reciprocating mechanism components, only few of them look into their interaction. One of them is Kim, T.-J. [18]. Nevertheless, the shaft misalignment was not cited by this author, and his study was carried out using a constant crankshaft angular velocity. Later on Chieh, H. [19] researched in his Ph.D. thesis a complete analysis of the bearing system in a reciprocating compressor. However, the inertial terms in the secondary movement directions were not taken into account, and the crankshaft angular velocity was also constant. Both Kim, T,-J. and Chieh, H. use the Gümbel boundary condition to treat the cavitation phenomena.

This paper aims to study the piston and crankshaft secondary movements and their interaction with each other, using a non-constant crankshaft angular velocity. Moreover, the crankshaft misalignment and the inertial forces in the secondary movement directions are also considered.

First, section 2 presents the mathematical formulation in which the numerical model is based. Section 3 shows the algorithm and the numerical techniques used to discretize and solve the equations presented in the previous section. The results are presented in section 4 and they have been divided into three parts. The first part contains the main proves used to verify and validate the numerical model. The second part presents two sensitivity studies to analyse the relevance of the inertial forces in the secondary movement directions and the effect of the non-constant angular velocity, respectively. The third part is composed of a set of parametric studies carried out to study the impact of different geometrical parameters in the stability and the friction power losses of the lubrication elements, and the compressor power consumption. Finally, section 5 shows the research conclusions.

Nomenclature

Geometry parameters

r	Radius
D	Diameter
L	Length
c	Clearance
e	Eccentricity
h	Distance between surfaces
o	Offset
G	Gravity centre

Mechanism locations

A	Connecting-rod pin connection with piston
B	Connecting-rod pin connection with crankshaft
C	Main bearing centre
D	Secondary bearing centre
O	Gravity centre of the crankshaft projected in its rotation axis

Kinematic parameters

v	Lineal velocity
a	Lineal acceleration

Dynamic parameters

p	Pressure
P	Power
F	Force
T	Torque
m	Mass
I	Inertia
k	Friction coefficient
H	Angular momentum

Superscripts

$\dot{\square}$	First time derivative
$\ddot{\square}$	Second time derivative
*	Dimensionless variable
n,n+1	Previous and next time instants

Subscripts

p	Piston
cr	Connecting-rod
cs	Crankshaft
wp	Wrist-pin
mb	Main bearing
sb	Secondary bearing
be	Bearing
h	Hydrodynamic
fr	Friction
g	Gas
t	Top
b	Bottom
cc	Compression chamber
M	Motor
k	Iteration number

Greek symbols

θ	Crankshaft angle
α	Connecting-rod angle
α_o	Connecting-rod angle when the piston is in its farthest position from the crankshaft
λ	Piston tilt angle in xy plane
δ	Crankshaft tilt angle in zx plane
γ	Crankshaft tilt angle in yz plane
ε	Dimensionless eccentricity
ϕ	Crankshaft mass eccentricity angle
φ	Local angle around a lubrication element
μ	Oil viscosity
ϑ	Every unknown in the global algorithm Fig. 6
ξ	Equivalent to $\pi + \theta - \phi$
ω	Angular velocity
ϵ	Numerical convergence criterion in the global algorithm

2. Mathematical Model

The mathematical formulation that defines the kinematic and dynamic behaviour of a reciprocating compressor mechanism is presented in this section. Fig. 1 shows a reciprocating compressor scheme, illustrating all the geometrical parameters. Gravity acts on z-direction.

The content of this section has been divided into three parts which are (i) the kinematic formulation, (ii) the dynamic formulation and (iii) the lubrication formulation.

2.1. Kinematic Formulation

The kinematic of the mechanism is based on the relation between the angles and the gravity centre motion the piston and the connecting-rod elements. Eq. (1) defines the connecting-rod angle (α) as function of the crankshaft angle (θ), as well as its first and second time derivatives.

$$\begin{aligned} \alpha &= \arcsin\left(\frac{r_{cs}\sin\theta + o_{cs}}{L_{cr}}\right) \\ \dot{\alpha} &= J_{\alpha_2}\dot{\theta} \\ \ddot{\alpha} &= J_{\alpha_1}\dot{\theta}^2 + J_{\alpha_2}\ddot{\theta} \end{aligned} \tag{1}$$

Where:

$$J_{\alpha_1} = -\frac{r_{cs}\sin\theta}{L_{cr}\cos\alpha} + \frac{r_{cs}^2\cos^2\theta\sin\alpha}{L_{cr}^2\cos^3\alpha} \quad J_{\alpha_2} = \frac{r_{cs}\cos\theta}{L_{cr}\cos\alpha} \tag{2}$$

2.1.1. Piston

When the piston is in its farthest position from the crankshaft, the angle α is defined by Eq. (3).

$$\alpha_o = \arcsin\left(\frac{o_{cs}}{L_{cr} + r_{cs}}\right) \tag{3}$$

The Eq. (4), Eq. (5) and Eq. (6) describe the position, velocity and acceleration of the piston gravity centre (G_p) on the x direction.

$$x_{G_p} = -L_{cr}\cos\alpha - r_{cs}\cos\theta \tag{4}$$

$$\dot{x}_{G_p} = v_p = \dot{\theta}\left(r_{cs}\sin\theta + J_{p_2}\right) \tag{5}$$

$$\ddot{x}_{G_p} = (r_{cs}\cos\theta + J_{p_1})\dot{\theta}^2 + (r_{cs}\sin\theta + J_{p_2})\ddot{\theta} \tag{6}$$

Where:

$$J_{p_1} = J_{\alpha_1} L_{cr} \sin\alpha + \frac{r_{cs}\cos^2\theta}{L_{cr}\cos\alpha} \quad J_{p_2} = J_{\alpha_2} L_{cr} \sin\alpha \tag{7}$$

2.1.2. Connecting-Rod

The position and acceleration in both axes of the connecting-rod gravity centre (G_{cr}) are expressed by the equations Eq. (8), Eq. (9), Eq. (10) and Eq. (11), respectively.

$$x_{G_{cr}} = -L_{G_{cr}}\cos\alpha - r_{cs}\cos\theta \tag{8}$$

$$y_{G_{cr}} = r_{cs}\sin\theta - L_{G_{cr}}\sin\alpha \tag{9}$$

$$\begin{aligned} \ddot{x}_{G_{cr}} = & \left(r_{cs}\cos\theta + \left(\frac{L_{G_{cr}}}{L_{cr}}\right) J_{p_1}\right)\dot{\theta}^2 \\ & + \left(r_{cs}\sin\theta + \left(\frac{L_{G_{cr}}}{L_{cr}}\right) J_{p_2}\right)\ddot{\theta} \end{aligned} \tag{10}$$

$$\begin{aligned} \ddot{y}_{G_{cr}} = & -r_{cs}\sin\theta\left(1 - \frac{L_{G_{cr}}}{L_{cr}}\right)\dot{\theta}^2 \\ & + r_{cs}\cos\theta\left(1 - \frac{L_{G_{cr}}}{L_{cr}}\right)\ddot{\theta} \end{aligned} \tag{11}$$

2.2. Dynamic Formulation

This part presents the dynamic equations used to calculate the main and secondary motion of each component of the reciprocating mechanism.

2.2.1. Piston

First, Fig. 2a represents the piston free body diagram. Using this diagram, the equations that describe the piston dynamics can be obtained.

$$F_g + F_{p_{fr}} - F_{A_x} = \left(m_p + m_{wp_p}\right)\ddot{x}_{G_p} \tag{12}$$

$$F_{p_h} - F_{A_y} = \left(m_p + m_{wp_p}\right)\ddot{y}_{G_p} \tag{13}$$

$$T_{p_{fr}} + T_{p_h} - T_{A_{fr}} = -I_{p_z}\ddot{\lambda} \tag{14}$$

Only the x and y linear movements and the z rotation are studied in the piston case. The term F_g is the force produced by the refrigerant when it is being compressed. It is calculated as $F_g = \pi r_p^2 (p_{cc} - p_{shell})$, where p_{cc} and p_{shell} are the instantaneous pressures in the compression chamber and the shell, respectively. Both pressures have a numerical origin and they are presented in Fig.3.

The piston secondary motion (Fig. 2b) has been calculated by using Eq. (13) and Eq. (14). In this work, the secondary movements have been defined as function of the top ($\varepsilon_{i_t} = e_{i_t}/c_i$) and bottom ($\varepsilon_{i_b} = e_{i_b}/c_i$) dimensionless eccentricities of each lubrication element, which are denoted as i. They are the cylinder-piston cavity (p), the main bearing (mb) and the secondary bearing (sb). Specifically in the cylinder-piston case, the $\ddot{y}_{G_p}$ and $\ddot{\lambda}$ are defined as Eq. (16).

$$y_{G_p} = c_p \left(\varepsilon_{p_{t_y}} - \left(\frac{\varepsilon_{p_{t_y}} - \varepsilon_{p_{b_y}}}{L_p} \right) L_{G_p} \right) \qquad \lambda = c_p \left(\frac{\varepsilon_{p_{t_y}} - \varepsilon_{p_{b_y}}}{L_p} \right) \tag{15}$$

$$\ddot{y}_{G_p} = c_p \, \dot{\theta}^2 \left(\ddot{\varepsilon}_{p_{t_y}} - \left(\frac{\ddot{\varepsilon}_{p_{t_y}} - \ddot{\varepsilon}_{p_{b_y}}}{L_p} \right) L_{G_p} \right) \qquad \ddot{\lambda} = c_p \, \dot{\theta}^2 \left(\frac{\ddot{\varepsilon}_{p_{t_y}} - \ddot{\varepsilon}_{p_{b_y}}}{L_p} \right) \tag{16}$$

2.2.2. Connecting-Rod

The connecting-rod free body diagram is shown in Fig. 4. The connecting-rod dynamics is defined by Eq. (17), Eq. (18) and Eq. (19).

$$-F_{B_x} + F_{A_x} = m_{cr} \ddot{x}_{Gcr} \tag{17}$$

$$-F_{B_y} + F_{A_y} = m_{cr} \ddot{y}_{Gcr} \tag{18}$$

$$\begin{aligned} &F_{A_x} (L_{cr} - L_{G_{cr}}) \sin\alpha - F_{A_y} (L_{cr} - L_{G_{cr}}) \cos\alpha \\ &+F_{B_x} L_{G_{cr}} \sin\alpha - F_{B_y} L_{G_{cr}} \cos\alpha + T_{A_{fr}} - T_{B_{fr}} = I_{cr_z} \ddot{\alpha} \end{aligned} \tag{19}$$

The friction torques on the connecting-rod pins are calculated using the experimental correlations defined by Eq. (20) and Eq. (21).

$$T_{A_{fr}} = -sgn(\dot{\alpha}) \, k_A r_A \left(|F_{A_x}| + \left| F_{A_y} \right| \right) \tag{20}$$

$$T_{B_{fr}} = k_B r_B \left(|F_{B_x}| + \left| F_{B_y} \right| \right) \tag{21}$$

Where k_A and k_B represent experimental friction factors at each connecting-rod pin, while r_A and r_B refer to their internal radius.

Note here how the x and y linear motion and z rotation are considered. The secondary motion of the connecting-rod are not studied in this work.

2.2.3. Crankshaft

The crankshaft free body diagram is shown in Fig. 5b and Fig. 5a. The crankshaft sum of forces is presented in Eq. (22), and is calculated only on the x and y axes. The z linear movement is not studied as a thrust bearing fixes the crankshaft on this direction.

$$\sum \vec{F}_{cs} = m_{cs}\vec{a}_{Gcs} \tag{22}$$

The acceleration of the crankshaft gravity centre ($\vec{a}_{Gcs}$) is equal to Eq. (23).

$$\vec{a}_{G_{cs}} = \vec{a}_O + \vec{\omega}_{cs} \times \vec{\omega}_{cs} \times \overrightarrow{OG}_{cs} + \vec{\dot{\omega}}_{cs} \times \overrightarrow{OG}_{cs} \tag{23}$$

$$\begin{aligned} \vec{a}_{G_{cs}} = \begin{pmatrix} \ddot{x}_O \\ \ddot{y}_O \\ 0 \end{pmatrix} + \begin{pmatrix} \dot{\gamma} \\ \dot{\delta} \\ \dot{\theta} \end{pmatrix} \times \left(\begin{pmatrix} \dot{\gamma} \\ \dot{\delta} \\ \dot{\theta} \end{pmatrix} \times \begin{pmatrix} r_{G_{cs}} \cos\xi \\ r_{G_{cs}} \sin\xi \\ 0 \end{pmatrix} \right) \\ + \begin{pmatrix} \ddot{\gamma} - \dot{\delta}\dot{\theta} \\ \ddot{\delta} + \dot{\gamma}\dot{\theta} \\ \ddot{\theta} \end{pmatrix} \times \begin{pmatrix} r_{G_{cs}} \cos\xi \\ r_{G_{cs}} \sin\xi \\ 0 \end{pmatrix} \end{aligned} \tag{24}$$

The angle ξ is defined as $\pi + \theta - \phi$ and the terms $\ddot{x}_O$, $\ddot{y}_O$, $\ddot{\gamma}$ and $\ddot{\delta}$ are expressed as function of each journal bearing dimensionless eccentricity accelerations by Eq. (25).

$$\begin{aligned} \ddot{x}_O &= c_{cs}\,\dot{\theta}^2 \left(\ddot{\varepsilon}_{sb_x} - \left(\frac{\ddot{\varepsilon}_{mb_x} - \ddot{\varepsilon}_{sb_x}}{L_{be}} \right) L_{G_{sb}} \right) \\ \ddot{y}_O &= c_{cs}\,\dot{\theta}^2 \left(\ddot{\varepsilon}_{sb_y} - \left(\frac{\ddot{\varepsilon}_{mb_y} - \ddot{\varepsilon}_{sb_y}}{L_{be}} \right) L_{G_{sb}} \right) \\ \ddot{\delta} &= c_{cs}\,\dot{\theta}^2 \left(\frac{\ddot{\varepsilon}_{sb_x} - \ddot{\varepsilon}_{mb_x}}{L_{be}} \right) \\ \ddot{\gamma} &= c_{cs}\,\dot{\theta}^2 \left(\frac{\ddot{\varepsilon}_{mb_y} - \ddot{\varepsilon}_{sb_y}}{L_{be}} \right) \end{aligned} \tag{25}$$

Where c_{cs} represents the clearance of the main and secondary bearings, which are considered equal.

Only taking into consideration the permitted movements of the crankshaft, the Eq. (23) is expressed as:

$$\vec{a}_{G_{cs}} = \underbrace{\begin{pmatrix} \ddot{x}_O \\ \ddot{y}_O \end{pmatrix}}_{\vec{a}_O} + \underbrace{\begin{pmatrix} -r_{G_{cs}}\dot{\theta}^2\cos\xi \\ -r_{G_{cs}}\dot{\theta}^2\sin\xi \end{pmatrix}}_{\vec{a}_n} + \underbrace{\begin{pmatrix} -r_{G_{cs}}\ddot{\theta}\sin\xi \\ r_{G_{cs}}\ddot{\theta}\cos\xi \end{pmatrix}}_{\vec{a}_a} + \underbrace{\begin{pmatrix} r_{G_{cs}}\left(-\dot{\delta}^2\cos\xi + \dot{\delta}\dot{\gamma}\sin\xi\right) \\ r_{G_{cs}}\left(-\dot{\gamma}^2\sin\xi + \dot{\delta}\dot{\gamma}\cos\xi\right) \end{pmatrix}}_{\vec{a}_{SM}} \tag{26}$$

The $\vec{a}_{SM}$ is assumed negligible as it is composed by the square of the crankshaft secondary angular velocities, which are relatively insignificant. Hence, the sum of forces on the crankshaft free solid diagram can be defined as Eq. (27).

$$\vec{F}_B + \vec{F}_{mb} + \vec{F}_{sb} - \underbrace{m_{cs}\vec{a}_n}_{\vec{F}_{cs_{I_n}}} - \underbrace{m_{cs}\vec{a}_a}_{\vec{F}_{cs_{I_a}}} - \underbrace{m_{cs}\vec{a}_O}_{\vec{F}_{cs_I}} = 0 \tag{27}$$

Where:

$$\frac{1}{m_{cs}}\left(F_{B_x} + F_{mb_x} + F_{sb_x}\right) + r_{G_{cs}}\left(\dot{\theta}^2\cos\xi + \ddot{\theta}\sin\xi\right) - c_{cs}\,\dot{\theta}^2\left(\ddot{\varepsilon}_{sb_x} - \left(\frac{\ddot{\varepsilon}_{mb_x} - \ddot{\varepsilon}_{sb_x}}{L_{be}}\right)L_{G_{sb}}\right) = 0 \tag{28}$$

$$\frac{1}{m_{cs}}\left(F_{B_y} + F_{mb_y} + F_{sb_y}\right) + r_{G_{cs}}\left(\dot{\theta}^2\sin\xi - \ddot{\theta}\cos\xi\right) - c_{cs}\,\dot{\theta}^2\left(\ddot{\varepsilon}_{sb_y} - \left(\frac{\ddot{\varepsilon}_{mb_y} - \ddot{\varepsilon}_{sb_y}}{L_{be}}\right)L_{G_{sb}}\right) = 0 \tag{29}$$

Furthermore, the crankshaft angular momentum defined by Eq. (30) is also needed to calculate the crankshaft angular acceleration, velocity and position.

$$\sum \vec{T}_{G_{cs}} = \frac{\mathrm{d}\vec{H}_{G_{cs}}}{\mathrm{d}t} \tag{30}$$

In this case the rotation movements are taken into account on the three coordinate axes. The angular momentum ($\vec{H}_{G_{cs}}$) is defined as $\bar{I}_{G_{cs}}\vec{\omega}_{cs}$. The angular momentum can be expressed as Eq. (31).

$$\overrightarrow{G_{cs}B} \times \vec{F}_B + \vec{T}_{B_{fr}} + \vec{T}_{mb_{G_{cs}}} + \vec{T}_{sb_{G_{cs}}} - \vec{T}_M = \frac{\mathrm{d}\vec{H}_{G_{cs}}}{\mathrm{d}t} \tag{31}$$

The term $\vec{T}_M$ represents the electric motor torque. This is obtained from Rigola's [13] study (experimental data). The torques produced by the journal bearings are denoted as $\vec{T}_{mb_{G_{cs}}}$ and $\vec{T}_{sb_{G_{cs}}}$, while $\mathrm{d}\vec{H}_{G_{cs}}/\mathrm{d}t$ represents the crankshaft inertial torque. These terms are defined in the Eq.(32), Eq.(33) and Eq.(34), respectively.

$$\vec{T}_{mb_{G_{cs}}} = \vec{T}_{mb_C} + \overrightarrow{G_{cs}C} \times \vec{F}_{mb} + \vec{T}_{mb_{fr}} \tag{32}$$

$$\vec{T}_{sb_{G_{cs}}} = \vec{T}_{sb_D} + \overrightarrow{G_{cs}D} \times \vec{F}_{sb} + \vec{T}_{sb_{fr}} \tag{33}$$

$$\frac{\mathrm{d}\vec{H}_{G_{cs}}}{\mathrm{d}t} = \begin{pmatrix} I_{cs_x}\ddot{\gamma} - I_{cs_y}\dot{\delta}\dot{\theta} \\ I_{cs_y}\ddot{\delta} + I_{cs_x}\dot{\gamma}\dot{\theta} \\ I_{cs_z}\ddot{\theta} \end{pmatrix} \tag{34}$$

Where, $\vec{T}_{mb_C}$ and $\vec{T}_{sb_D}$ are the misalignment torques, while $\vec{T}_{mb_{fr}}$ and $\vec{T}_{sb_{fr}}$ represents the journal bearing friction torques. The distance vectors are defined by Eq.(35).

$$\begin{aligned} \overrightarrow{G_{cs}C} &= \begin{pmatrix} -r_{G_{cs}}\cos\xi \\ -r_{G_{cs}}\sin\xi \\ -L_{G_{mb}} \end{pmatrix} \\ \overrightarrow{G_{cs}D} &= \begin{pmatrix} -r_{G_{cs}}\cos\xi \\ -r_{G_{cs}}\sin\xi \\ -L_{G_{sb}} \end{pmatrix} \\ \overrightarrow{G_{cs}B} &= \begin{pmatrix} -r_{cs}\cos\theta - r_{G_{cs}}\cos\xi \\ r_{cs}\sin\theta - r_{G_{cs}}\sin\xi \\ -L_{G_{cs}} \end{pmatrix} \end{aligned} \tag{35}$$

Finally, the crankshaft momentum equations on each coordinate axis are

expressed by Eq. (36), Eq. (37) and Eq. (38).

$$\begin{aligned} &F_{B_y} L_{G_{cs}} + F_{mb_y} L_{G_{mb}} + F_{sb_y} L_{G_{sb}} + T_{mb_{C_x}} + T_{sb_{D_x}} \\ &-c_{cs}\,\dot{\theta}^2 \left(I_x \left(\frac{\ddot{\varepsilon}_{mb_y} - \ddot{\varepsilon}_{sb_y}}{L_{be}} \right) - I_y \left(\frac{\dot{\varepsilon}_{sb_x} - \dot{\varepsilon}_{mb_x}}{L_{be}} \right) \right) = 0 \end{aligned} \tag{36}$$

$$\begin{aligned} &-F_{B_x} L_{G_{cs}} - F_{mb_x} L_{G_{mb}} - F_{sb_x} L_{G_{sb}} + T_{mb_{C_y}} + T_{sb_{D_y}} \\ &-c_{cs}\,\dot{\theta}^2 \left(I_y \left(\frac{\ddot{\varepsilon}_{sb_x} - \ddot{\varepsilon}_{mb_x}}{L_{be}} \right) + I_x \left(\frac{\dot{\varepsilon}_{mb_y} - \dot{\varepsilon}_{sb_y}}{L_{be}} \right) \right) = 0 \end{aligned} \tag{37}$$

$$\begin{aligned} -r_{cs} \left(F_{B_y} \cos\theta + F_{B_x} \sin\theta \right) + T_{mb_{fr}} + T_{sb_{fr}} + T_{B_{fr}} \\ -T_{M_z} + r_{G_{cs}} \left(F_{B_x} + F_{mb_x} + F_{sb_x} \right) \sin\xi \\ -r_{G_{cs}} \left(F_{B_y} + F_{mb_y} + F_{sb_y} \right) \cos\xi - I_z \ddot{\theta} = 0 \end{aligned} \tag{38}$$

Specifically, Eq. (38) is used to calculate the macroscopic motion of the reciprocating mechanism, while Eq. (28), Eq. (29), Eq. (36), Eq. (37) are needed to determine the crankshaft secondary movements.

2.3. Lubrication Formulation

The hydrodynamic and friction reactions of the different lubrication elements are necessary to determine the reciprocating compressor behaviour. These reactions depend on the pressure distribution around each lubrication element, which is obtained by solving the well-known Reynolds equation. It is worth noting here that the roughness and asperities are not taken into account in this equation, because the condition $h/\sigma \geq 3$ is considered satisfied. Where h is the local distance between surfaces and σ is the roughness deviation of the surface. Authors as Patir, N. and Cheng, H.S. [20] or Zhu, D. et al. [9] demonstrated that the roughness and asperities effects were not necessary to be considered when this condition was satisfied.

2.3.1. Piston

The Reynolds equation used to determine the pressure distribution around the cylinder-piston cavity is expressed by Eq. (39).

$$\frac{1}{r_p^2} \frac{\partial}{\partial \varphi} \left(h_p^3 \frac{\partial p}{\partial \varphi} \right) + \frac{\partial}{\partial x} \left(h_p^3 \frac{\partial p}{\partial x} \right) = 12 \mu_p \left(\frac{v_p}{2} \frac{\partial h_p}{\partial x} + \frac{\partial h_p}{\partial t} \right) \tag{39}$$

The term v_p refers to the piston velocity. The geometric variable h_p represents the local film thickness of the cylinder-piston cavity and is defined by Eq. (40), as the piston skirt is cylindrical on the whole (e.g. barrel profiles are not considered in this study). This term only depends on the top and bottom piston dimensionless eccentricities on the y-axis, as it is the only secondary movement allowed by the piston.

$$h_p = c_p \left(1 - \left(\varepsilon_{p_{t_y}} - \left(\frac{\varepsilon_{p_{t_y}} - \varepsilon_{p_{b_y}}}{L_p}\right) x\right) \cos\varphi\right) \tag{40}$$

The hydrodynamic forces and torques produced by the pressure distribution around the cylinder-piston cavity are calculated using Eq. (41) and Eq. (42), respectively.

$$F_{p_h} = -\int_0^{L_p} \int_0^{2\pi} p\left(\varphi, x\right) \cos\varphi \, r_p \mathrm{d}\varphi \mathrm{dx} \tag{41}$$

$$T_{p_h} = -\int_0^{L_p} \int_0^{2\pi} p\left(\varphi, x\right) \cos\varphi \left(x_{ij} - L_{wp_p}\right) r_p \mathrm{d}\varphi \mathrm{dx} \tag{42}$$

The term x_{ij} defines the distance from the top of the piston to a piston mesh node on the axial direction (x). The force and the torque produced by the friction between the piston surface and the fluid film are defined by Eq. (43) and Eq. (44), respectively.

$$F_{p_{fr}} = -\int_0^{L_p} \int_0^{2\pi} \left(\frac{h_p}{2}\frac{\partial p}{\partial x} + \mu_p \frac{v_p}{h_p}\right) r_p \mathrm{d}\varphi \mathrm{dx} \tag{43}$$

$$T_{p_{fr}} = \int_0^{L_p} \int_0^{2\pi} \left(\frac{h_p}{2}\frac{\partial p}{\partial x} + \mu_p \frac{v_p}{h_p}\right) \cos\varphi r_p \mathrm{d}\varphi \mathrm{dx} \tag{44}$$

The cavitation phenomenon appears on the piston. When it happens, a linear interpolation between the compression chamber pressure (p_{cc}) and the shell pressure (p_{shell}) is used to substitute the negative values.

2.3.2. Crankshaft

Eq. (45) represents the Reynolds equation used to calculate the pressure distribution around the journal bearings.

$$\frac{1}{r_i^2}\frac{\partial}{\partial\varphi}\left(h_i^3 \frac{\partial p_i}{\partial\varphi}\right) + \frac{\partial}{\partial z}\left(h_i^3 \frac{\partial p_i}{\partial z}\right) = 12\mu_{cs}\left(\frac{\dot{\theta}}{2}\frac{\partial h_i}{\partial\varphi} + \frac{\partial h_i}{\partial t}\right) \tag{45}$$

The subscript i denotes the journal bearing which is evaluated (mb or sb) and $\dot{\theta}$ represents the crankshaft angular velocity on the z axis. In this case, the term h_i is defined by Eq. (46) and represents the film thickness of the main or secondary bearing cavity. This variable depends on the top and bottom dimensionless eccentricities on the x and y axis.

$$h_i = c_{cs}\left(1 - \left(\varepsilon_{i_{t_x}} - \left(\frac{\varepsilon_{i_{t_x}} - \varepsilon_{i_{b_x}}}{L_i}\right) z\right)\cos\varphi + \left(\varepsilon_{i_{t_y}} - \left(\frac{\varepsilon_{i_{t_y}} - \varepsilon_{i_{b_y}}}{L_i}\right) z\right)\sin\varphi\right) \tag{46}$$

As the crankshaft is considered a rigid body, the main and secondary bearings share the same tilt angle. These angles in the zx and yz planes are defined in Eq. (47) and Eq. (48), respectively. These equalities can be easily understood observing Fig.5c.

$$\delta = -c_{cs}\left(\frac{\varepsilon_{i_{t_x}} - \varepsilon_{i_{b_x}}}{L_i}\right) = -c_{cs}\left(\frac{\varepsilon_{mb_x} - \varepsilon_{sb_x}}{L_{be}}\right) \tag{47}$$

$$\gamma = c_{cs}\left(\frac{\varepsilon_{i_{t_y}} - \varepsilon_{i_{b_y}}}{L_i}\right) = c_{cs}\left(\frac{\varepsilon_{mb_y} - \varepsilon_{sb_y}}{L_{be}}\right) \tag{48}$$

The hydrodynamic forces and misalignment torques produced by the pressure distribution around the journal bearings are calculated using Eq. (49) and Eq. (50), respectively.

$$\vec{F_i} = -\int_0^{L_i}\int_0^{2\pi} p\left(\varphi, z\right)\left(\cos\varphi, \sin\varphi, 0\right) r_i \mathrm{d}\varphi\mathrm{d}z \tag{49}$$

$$\vec{T_i} = \int_0^{L_i}\int_0^{2\pi} p\left(\varphi, z\right)\left(\sin\varphi, -\cos\varphi, 0\right)\left(z_{ij} - 0.5L_i\right) r_i \mathrm{d}\varphi\mathrm{d}z \tag{50}$$

The term z_{ij} represents the distance from the centre of the bearing to the crankshaft mesh node. The friction torque is evaluated on the bearings using Eq. (51).

$$T_{i_{fr}} = \int_0^{L_i}\int_0^{2\pi}\left(\frac{h_i}{2r_i}\frac{\partial p}{\partial\varphi} + \mu_{cs}\frac{\dot{\theta} r_i}{h_i}\right) r_i \mathrm{d}\varphi\mathrm{d}z \tag{51}$$

The Gümbel boundary condition is used to deal with the journal bearings cavitation problem.

3. Numerical Procedure

This section presents the global resolution algorithm (Fig. 6) and the numerical techniques used to properly solve the equations described in the previous section.

The algorithm is based on a temporal implicit formulation organised in three sub-iterative blocks: the main motion of the reciprocating mechanism (Block 1), the piston secondary motion (Block 2), and the crankshaft secondary motion (Block 3). These procedures are inter-dependent. Thus, they must be calculated iteratively in order to couple them well.

Initially, the crank angle is zero and its angular velocity is known. The eccentricities of the lubrication elements as well as their rate of change are assumed zero at the first calculation. The main dimensions, weights, physical properties and geometry of the full mechanism are considered input data. The instantaneous pressure of the refrigerant fluid inside the compression chamber is also assumed as known data. This information can be obtained by means of other numerical approaches that address the fluid dynamics of the refrigerant gas over all the different compressor phases. In this work, the instantaneous pressure in the compression chamber, as well as the electric motor torque, are obtained from Rigola's [13] study.

3.1. Block 1: Main motion of the reciprocating-mechanism

This procedure is focused on the macroscopic motion of the elements of the reciprocating mechanism. In particular, it is aimed to obtain the instantaneous values of the angular acceleration of the crankshaft ($\ddot{\theta}$) and the force reactions on the connecting-rod ($\vec{F}_A$, $\vec{F}_B$). Other parameters such as the piston velocity (v_p), the angular velocity ($\dot{\theta}$) and the crank position (θ) are derived from these data.

The macroscopic motion is driven by Eq. (12), Eq. (17), Eq. (18), Eq. (19) and Eq. (38). These equations are expressed as function of the crankshaft angular acceleration ($\ddot{\theta}$) and the force reactions on the connecting-rod ($\vec{F}_A$, $\vec{F}_B$), by using the kinematic relations presented in subsection 2.1.

A Runge-Kutta/Ralston second order implicit scheme method is applied for advancing the time variable. The resulting system of equations is resolved by means of the Lower-Upper (LU) solver. To use this approach the values of $F_{p_{fr}}^{n+1}$, $F_{mb_x}^{n+1}$, $F_{mb_y}^{n+1}$, $T_{mb_{fr}}^{n+1}$, $F_{sb_x}^{n+1}$, $F_{sb_y}^{n+1}$ and $T_{sb_{fr}}^{n+1}$ must be supposed. These data is calculated in the further resolution of the piston and the crankshaft secondary motions.

3.2. Block 2: Piston secondary motion

This procedure is aimed to obtain the hydrodynamic and friction reactions on the piston element. For doing this, the secondary motion of the piston is resolved.

This motion is mathematically expressed in Eq. (13) and Eq. (14). These equations depend on the piston gravity centre accelerations in the secondary movement directions ($\ddot{y}_{G_p}, \ddot{\lambda}$), which are defined in terms of the top and bottom linear accelerations of the piston ($\ddot{\varepsilon}_{p_t}, \ddot{\varepsilon}_{p_b}$) in Eq.(16).

A first order Euler implicit scheme method is applied for advancing the time variable. The resulting system of equations is solved through a Newton-Raphson (NR) based method. The hydrodynamic and friction reactions depend on the pressure distribution around the cylinder-piston cavity. That pressure is mathematically modelled by means of the Reynolds equation, which is solved using a Finite Volume Method (FVM) strategy. The system of equations arising from the FVM discretization is solved by means of the Cholesky solver.

It is necessary to emphasise that this procedure depends on θ^{n+1}, $\dot{\theta}^{n+1}$, $F_{A_y}^{n+1}$ and $T_{A_{fr}}^{n+1}$. These data are provided by Block 1 procedure, explained in subsection 3.1. Hence, the piston secondary motion is preceded by Block 1.

3.3. Block 3: Crankshaft secondary motion

This procedure is aimed to obtain the hydrodynamic and friction reactions on the crankshaft element. For doing this, the secondary motion of the crankshaft is resolved.

This motion is mathematically described by Eq. (28), Eq. (29), Eq. (36) and Eq. (37). These equations depend on the crankshaft gravity centre accelerations in the secondary movement directions ($\ddot{x}_O, \ddot{y}_O, \ddot{\gamma}, \ddot{\delta}$), which are defined in terms of the main and secondary linear accelerations of the crankshaft ($\ddot{\varepsilon}_{mb_x}, \ddot{\varepsilon}_{mb_y}, \ddot{\varepsilon}_{sb_x}, \ddot{\varepsilon}_{sb_y}$) in Eq. (25).

In a similar way as in Block 2, a first order Euler implicit scheme method is applied for advancing the time variable. The resulting system of equations is solved using Newton-Raphson (NR) based method, too. The hydrodynamic and friction reactions are also calculated through the resolution of the Reynolds equation using a FVM discretization in each bearing.

Again, this procedure depends on data that is calculated in Block 1 procedure. In particular, the crankshaft motion depends on θ^{n+1}, $\dot{\theta}^{n+1}$, $F_{B_x}^{n+1}$, $F_{B_y}^{n+1}$ and $T_{B_{fr}}^{n+1}$. For this reason, the part is preceded by Block 1 in the global resolution algorithm.

4. Results and discussions

The reciprocating compressor mechanism simulations are based on the design parameters presented in Table 1. This section is divided into three parts which contain: (i) a group of studies to verify and validate the developed code; (ii) a sensitivity analysis of the inertial forces on the secondary movement direction first and the crankshaft angular acceleration later, for evaluating their impact on the overall behaviour of the reciprocating mechanism; (iii) and a set of parametric studies.

4.1. Verification and validation results

4.1.1. Verification results

Different results are presented analysing two spatial and one time discretization error studies. The assessment of the spatial discretization error is focused on the use of different meshes in the FVM based resolution of the Reynolds equation. Furthermore, the time discretization error is based on the use of different time integration steps for solving the overall mathematical model.

The first spatial discretization error study consists of analysing an aligned and static journal bearing. In particular, the bearing is uncoupled from the remain compressor components. The Sommerfeld number and the load angle have been evaluated for every tested mesh, using different eccentricities. In order to show the asymptotic tendency of the numerical solutions, the different results have been compared to those obtained with the $mesh_{80x80}$[1]. The average relative errors using the $mesh_{10x10}$ are lower than 9.2% for the Sommerfeld number and 13% for the load angle. The errors for the $mesh_{20x20}$ are lower than 3.1% in both cases. Finally, the $mesh_{30x30}$ and the $mesh_{40x40}$ provide errors below 1.2% and 0.6% respectively. Thus, it is considered that the $mesh_{20x20}$ solves the lubrication phenomena in uncoupled journal bearings problem with an acceptable precision in a reasonable computational time.

The second spatial discretization error study is focused on the calculation of the crankshaft and the piston trajectories. Unlike the previous study, this is solving all the mechanism fully coupled. In this case, the asymptotic tendencies are obtained by comparison of every numerical solution to the

[1]The nomenclature $mesh_{NxM}$ is used to define the size of the uniform mesh, where N and M are the nodes in the circumferential and the axial direction, respectively

one obtained using the $mesh_{30x30}$. The relative errors with the $mesh_{10x10}$ are lower than 2.2% for the crankshaft trajectory while the errors for the $mesh_{20x20}$ are below 0.7%. In addition the average absolute difference of the piston trajectory is lower than $10^{-2}\mu m$ in all cases. Thus, according to these data the $mesh_{10x10}$ provides sufficient accuracy.

With regard to the time discretization error study, the different time steps are determined on the basis of the cyclic nature of the addressed problem. Namely, the whole crank rotation is divided in n equally separated time instants wherein the mechanism is solved. In that way, the time step is altered by changing the number of divisions, or just steps, the cycle is divided in. The study comprises different cases ranging from 100 to 800 steps. For verifying the asymptotic behaviour, all the numerical solutions have been compared with the results obtained with 800 steps. Using 100 steps the average relative errors are lower than 5% for both the main and the secondary bearing trajectories, using 200 steps the error is lower than 2.3% and using 400 steps the error is below 0.8%. Moreover, the average absolute errors of the piston trajectory are lower than $10^{-2}\mu m$ in all cases. Thus, according to this study the discretization of the crank cycle in 200 steps gives a sufficient adequate accuracy.

4.1.2. Validation results

The results obtained by the developed code are validated using the numerical results of several authors. These validations have been focused on the Reynolds Equation as it is essential to properly evaluate the secondary movements of the reciprocating mechanism.

In the literature, there are some analytical solutions regarding the Reynolds equation applied on the aligned journal bearings. The most famous are the infinitely long and short bearing cases, although their applicability is limited. More recently, another much less restrictive analytical solution has been developed by Sfyris, D. and Chasalevris, A. [21; 22]. This analytical solution, along with the numerical results obtained by Gertzos [5] and the results obtained by the developed code, are shown in Fig. 7. A good agreement is observed among the results, specifically with the code and Gertzos' results.

The analytical solution of Sfyris, D. and Chasalevris, A. [21; 22] can be also used to determine the pressure distribution of a journal bearing when it has a dimensionless eccentricity (ε) and a non-zero rate of change ($\dot{\varepsilon}$). A comparison of this analytical solution and the numerical code results is shown in Fig.8. A good concordance is observed.

The following numerical experiment shows the aligned journal bearing behaviour under dynamic loads. The results obtained by the developed code are compared with the experimental studies by Campbell et al. [1] and the numerical studies by Jones, G.J. [3] in Fig. 9. This figure shows a journal bearing trajectory during one cycle when different dynamic loads are applied. A close concordance between these trajectories is also observed.

Finally, the misaligned journal bearing behaviour is taken into consideration. A shaft misalignment produces misalignment torques on the journal bearing which tend to align the shaft again. These torques depend on the misalignment degree (D_m), the misalignment orientation (δ_{mis}) and the eccentricity of the journal bearing centre. All these parameters are defined by Wisbeck, H.J. [23]. As there is no analytical solution for misaligned journal bearing, this phenomenon has been studied numerically in the literature. Some of the authors who developed studies in this area are Wisbeck, H.J. [23] and Chieh, H.[19]. Their results have been used in Fig. 10 to validate the code. Once again, the results present a good agreement.

4.2. Sensitivity analysis

This section numerically concludes the influence of two physical phenomena in the compressor behaviour: (i) the relevance of the inertia in the secondary movement directions (piston and crankshaft), and (ii) the importance to take into account the oscillations of the crankshaft angular velocity.

4.2.1. Inertial Study

The computational cost of the numerical approach can be significantly reduced by means of simplification hypothesis. This study is aimed to investigate how the inertial forces in the secondary motion directions influence the compressor secondary motions. If these forces are not affecting the secondary movements, it can be assumed that the dynamics and the kinematics of the lubrication element can be uncoupled in the mathematical formulation. In this way the cost of the calculations can be reduced using appropriate numerical techniques.

To that end, two simulations have been carried out. The first one taking into account the inertial forces in the secondary motion directions and the other without considering them. The differences in the trajectories of the crankshaft and the piston have been calculated. The average relative differences (Fig. 11) in the crankshaft trajectory is lower than 4% and below 0.2% in the piston trajectory.

The differences are higher in the crankshaft because it is heavier than the piston. Even so, that difference is still low so that one can safely assume that the inertial terms do not affect the lubrication element trajectories, at least for the target compressor.

4.2.2. Crankshaft angular velocity study

The crankshaft angular velocity is not imposed in the current mathematical model, but it is derived from the inclusion of Eq. (38) into the dynamic balances. Because of this, the crankshaft angular velocity is not constant and their oscillations could affect the compressor secondary movements. These have been analysed through the piston and crankshaft trajectories with variable and constant angular velocity. Fig. 12 shows the oscillation of the crankshaft angular velocity and the crankshaft angular acceleration during one cycle. It can be seen that the difference between the maximum and the minimum angular velocity is approximately 1 Hz ($\approx 2\%$). The average angular velocity used to simulate the constant case is also shown in the figure (equal to $48.73\,Hz$).

The results show that the crankshaft trajectory presents an average relative difference lower than 0.65%, while the average absolute difference in the piston case is lower than 5e-3μm. Thus, the tiny differences prove that the oscillation effect is negligible in this case. Again, it does not mean that this phenomenon could not be important if other geometries were considered.

4.3. Parametric Studies

A set of parametric studies have been carried out to analyse the influence of different geometrical parameters in the stability and the friction power losses of each lubrication element, as well as in the compressor power consumption. The chosen parameters are (i) the angular position of the crankshaft mass eccentricity, (ii) the clearance of the piston and the crankshaft and (iii) the compressor offset. All these studies have been simulated using a $mesh_{10x10}$ and a number of steps equal to 200, as they provide sufficient accuracy (see 4.1.1).

4.3.1. Angular position of the crankshaft mass eccentricity (ϕ)

This section aims to analyse the influence of the angular position of the crankshaft mass eccentricity in the compressor behaviour. Preliminary results reveal that the crankshaft is the only element of the reciprocating mechanism affected by this parameter. Thus, the studies are focused on this element.

First, a maximum crankshaft stability point close to 270^o is observed in Fig. 13a, while the minimum is around 90^o. Specifically, the secondary bearing is more affected than the main bearing as it is closer to the crankshaft gravity centre. Moreover, Fig. 13b shows how the compressor power consumption remains practically invariable (small fluctuations) along ϕ. These consumption fluctuations are due to the fact that the angular position of the crankshaft mass eccentricity affects the bearing friction power losses. Therefore, if the angle ϕ is changed, the journal bearings stability can be improved without altering the consumption and the piston behaviour.

4.3.2. Clearances (c_p, c_{cs})

The clearance is an important geometrical parameter which affects the stability of the lubrication element and its friction power losses. The preliminary studies show that the clearance of one lubrication element does not alter the performance of the other lubrication elements, only its own. For this reason, the piston and the journal bearing clearances have been studied separately.

First, the effects of the piston clearance in the piston behaviour are commented. As shown in Fig. 14a, the maximum top eccentricity remains practically constant, while the maximum bottom eccentricity is increased. Thus, the piston is closer to the wall if its clearance is increased, which means a loss of stability. Instead, when the piston clearance increases, the friction power losses produced by the piston motion (Fig. 14a) decrease . These tendencies are not exactly the same as those observed by Prata, A.T. [11] and Kim, T.-J. [12]. The reason for this is that the piston stability is complex and it depends on several parameters.

Similarly to the piston case, the clearances of the journal bearings have also been studied. Fig. 14b shows how the crankshaft apparently loses stability and produces less friction power losses when the journal bearing clearances augment. This behaviour is also observed in the piston analysis although the trends are more pronounced in the crankshaft case.

4.3.3. Offset (o_{cs})

The compressor offset determines the distance in the y-direction between the points A and B (AB_y) along the compressor cycle (Fig. 4). An appropriate offset produces a decrease of AB_y during the compression stage, which is an interesting property. The shorter this distance during the compression stage is, the higher the compressor torque dedicated to produce the force in

the x-direction to compress the gas. This also means that the forces on the y-direction are smooth, improving the stability of the piston and crankshaft secondary movements. Moreover, the compressor power consumption decreases, as the average motor torque required to compress the gas is reduced (see Fig.15a). Consequently, the crankshaft angular velocity increases so that the crankshaft stability, the friction power losses and the flow rate pumped by the compressor augment.

These phenomena can be observed in Fig. 15b and Fig. 15c. The first figure shows the piston behaviour under different offsets. A maximum stability and a minimum friction power losses are identified. In the second figure it can be seen how an increase of the compressor offset improves the journal bearings stability, but it also produces more friction power losses. Both effects are related to the increase of the crankshaft angular velocity.

5. Conclusions

The current work describes the compressor mechanism behaviour based on the numerical resolution of several effects, which have been separately solved by other authors. The novelty of the present paper focuses on the capacity of coupling all these effects allowing to know the influence of different parameters from a global point of view. Hence, the developed model is a valuable tool to design reciprocating mechanisms as the compressor. It is not only able to predict the main motions of the different mechanism elements and their instantaneous behaviour over the cycle, but it also calculates their stability and their friction power losses. A great strength of the current work is the capability to evaluate all these features using different electric motors.

Two sensitivity analyses and a set of parametric studies have been carried out for assessing the modelling approach and better understanding of the compressor behaviour. First, the sensitivity analyses have concluded that neither the inertial forces in the directions of the secondary movements, nor the oscillations of the angular velocity affect the behaviour of the compressor studied in this research. Instead, the parametric studies have shown the high relevance of the selected parameters into the reciprocating compressor mechanism. The first parametric study reveals that the angular position of the crankshaft mass eccentricity affects the crankshaft stability and the friction power losses of their bearings (specially the second one). The angle ϕ, which provides the maximum stability without increasing the compressor power consumption, has been localised. The second parametric study exposes that the clearance of one lubrication element does not alter the performance of the other lubrication elements, only its own. Moreover, the piston stability as function of its clearance does not present the same tendency than other authors. This phenomenon can be explained to the fact that the piston stability is complex and it depends on several parameters. Finally, the last parametric study demonstrates the high influence of the offset on the compressor behaviour. This work has shown numerically that the compressor offset is able to improve the stability of the lubrication elements, reduces the electric motor torque, decreases the compressor power consumption and augments the flow rate pumped by the compressor. However, the friction power losses of the lubrication elements increase, due to an increase of the crankshaft angular average velocity.

Some other features could be included to extend the developed model. For example, an interesting experiment is the coupling of the reciprocating

mechanism with the fluid dynamics and the heat transfer of the refrigerant gas. In this context, the instantaneous pressure in the compression chamber would be calculated, instead of being imposed as a boundary condition. In addition, this would also enable the COP prediction in the basis of any other parameter. Another improvement is focused on the coupling of the distinct secondary movements. These movements are coupled by the dynamic formulation, so the kinematics of the secondary movements can only affect through the dynamic reactions which they produce. An improvement of the coupling grade between the secondary movements would be achieved through the calculation of the connecting-rod secondary movement in the existing model, as it could link the information of the piston and crankshaft secondary movements.

[1] S. O. Campbell, J., Love, P. P., Martin, F. A., Rafique, Bearings For Reciprocating Machinery: A Review of the Present State of Theoretical, Experimental and Service Knowledge, in: Proc. Instn Mech Engrs, 1967, pp. 51–74.

[2] Booker J. F., Dynamically-loaded journal bearings. Numerical application of the mobility method, J Lubric Technol Trans ASME 93 Ser F (1) (1971) 168–176.

[3] G. J. Jones, Crankshaft Bearings: Oil Film History, in: Proceedings of the 9th Leeds Lyon Symposium of Tribology, 1982, pp. 83–88.

[4] B. Yu, J. Sawicki, Comparison of Mobility Method and Mass Conservation Method in a Study of Dynamically Loaded Journal Bearings, International Journal of Rotating Machinery 8 (1) (2002) 71–79.

[5] K. Gertzos, P. Nikolakopoulos, C. Papadopoulos, CFD analysis of journal bearing hydrodynamic lubrication by Bingham lubricant, Tribology International 41 (12) (2008) 1190–1204. doi:10.1016/j.triboint.2008.03.002.

[6] D. F. Li, S. M. Rohde, H. A. Ezzat, An automotive piston lubrication model. (1982).

[7] M. C. Shaw, T. J. Nussdorfer, A Visual Study of Cylinder Lubrication, Tech. rep. (jan 1946). doi:10.4271/460084.

[8] A. B. Greene, Initial visual studies of piston-cylinder dynamic oil film behaviour, Wear 13 (4-5) (1969) 345–360.

[9] D. Zhu, H. Cheng, T. Arai, K. Hamai, Numerical analysis for piston skirts in mixed lubrication. part i: Basic modeling, Journal of Tribology 114 (3) (1992) 553–562.

[10] D. Zhu, Y.-Z. Hu, H. S. Cheng, T. Arai, K. Hamai, Numerical analysis for piston skirts in mixed lubrication - part ii: Deformation considerations, Journal of Tribology 115 (1) (1993) 125–133.

[11] A. T. Prata, J. R. S. Fernandes, F. Fagotti, Dynamic Analysis of Piston Secondary Motion for Small Reciprocating Compressors.pdf, ASME Transaction 122 (October) (2000) 752–760.

[12] T.-J. Kim, Dynamic analysis of a reciprocating compression mechanism considering hydrodynamic forces, KSME International Journal 17 (6) (2003) 844–853.

[13] J. Rigola, C. D. Pérez-Segarra, A. Oliva, Numerical simulation of the leakage through the radial clearance between piston and cylinder in hermetic reciprocating compressors., in: Proceedings of the International Conference of Compressors and their Systems, 2003, pp. 313–321.

[14] J. Rigola, C. D. Pérez-Segarra, A. Oliva, Numerical simulation of piston leakage over hermetic reciprocating compressors behavior, in: Institution of Mechanical Engineers - International Conference on Compressors and their Systems, 2009, pp. 375–384.

[15] J. Cho, S. Moon, A numerical analysis of the interaction between the piston oil film and the component deformation in a reciprocating compressor, Tribology International 38 (5) (2005) 459–468. doi:10.1016/j.triboint.2004.10.002.

[16] X. Meng, C. Fang, Y. Xie, Transient tribodynamic model of piston skirt-liner systems with variable speed effects, Tribology International 94 (2016) 640–651. doi:10.1016/j.triboint.2015.10.034.

[17] H. Liu, H. Xu, P. J. Ellison, Z. Jin, Application of Computational Fluid Dynamics and FluidStructure Interaction Method to the Lubrication Study of a RotorBearing System, Tribology Letters 38 (3) (2010) 325–336. doi:10.1007/s11249-010-9612-6.

[18] T.-J. Kim, J.-S. Han, Comparison of the Dynamic Behavior and Lubrication Characteristics of a Reciprocating Compressor Crankshaft in Both Finite and Short Bearing Models, Tribology Transactions 47 (1) (2004) 61–69. doi:10.1080/05698190490279029.

[19] H. Chieh, Modelagem E Análise Computacional Da Lubrificação Do Conjunto Eixo, Biela E Pistão Em Compressores Alternativos, Ph.D. thesis, Universidade Federal de Santa Catarina (2007).

[20] N. Patir, H. Cheng, An average flow model for determining effects of three-dimensional roughness on partial hydrodynamic lubrication, J Lubric Technol Trans ASME 100 (1 , Jan. 1978) (1978) 12–17.

[21] D. Sfyris, A. Chasalevris, An exact analytical solution of the Reynolds equation for the finite journal bearing lubrication, Tribology International 55 (2012) 46–58. doi:10.1016/j.triboint.2012.05.013.

[22] A. Chasalevris, D. Sfyris, Evaluation of the finite journal bearing characteristics, using the exact analytical solution of the Reynolds equation, Tribology International 57 (2013) 216–234. doi:10.1016/j.triboint.2012.08.011.

[23] H. Wisbeck, Uma Nova Metodologia de Solução para Sistemas de Mancais Radi, Ph.D. thesis, Universidade Federal de Santa Catarina (2000).

List of Tables

Piston			
Radius	r_p	13.5	mm
Length	L_p	21.0	mm
Clearance	c_p	5.0	μm
Dynamic viscosity	μ_p	4.0e-3	$Pa\,s$
Connecting-Rod			
Length	L_{cr}	42.0	mm
Crankshaft			
Radius	r_{cs}	8.7	mm
Offset	o_{cs}	3.0	mm
Gravity centre radius	$r_{G_{cs}}$	0.1	mm
Gravity centre angle	ϕ	0.0	deg
Distance between bearings	L_{be}	42.0	mm
Clearance	c_{cs}	9.0	μm
Dynamic viscosity	μ_{cs}	6.0e-3	$Pa\,s$
Main bearing			
Radius	r_{mb}	7.5	mm
Length	L_{mb}	10.0	mm
Position	$L_{G_{mb}}$	50.0	mm
Secondary bearing			
Radius	r_{sb}	7.5	mm
Length	L_{sb}	7.5	mm
Position	$L_{G_{sb}}$	8.0	mm

Table 1: Design parameters.

List of Figures

10 Dimensionless misalignment torques in the (a) x-direction a (T_x) and (b) y-direction T_y) as function of the misalignment degree (D_m) using different orientations (δ_{mis}). Comparison between the results obtained by Wisbeck, H.J. [23], and Chieh, H.[19] and the results obtained by the code.

11 Comparison of the (a) piston and (b) crankshaft trajectories during a compressor cycle when the inertial forces in the secondary motion directions are considered and when they are not. The detailed view shows the differences among the secondary bearing trajectories.

12 Crankshaft angular velocity ($\dot{\theta}$) and acceleration ($\ddot{\theta}$) along the compressor cycle (θ).

13 (a) Maximum dimensionless eccentricity (ε_{max}) of the main and secondary bearings and (b) compressor power consumption (P_{mec}) as function of the angular position of the crankshaft mass eccentricity (ϕ).

14 Friction power losses (P_{fr}) and maximum dimensionless eccentricities (ε_{max}) of (a) the piston as function of its clearance (c_p) and (b) the journal bearings as function of their clearances (c_{cs}).

15 (a) Average motor torque (T_m) and average angular velocity ($\dot{\theta}$) during a compressor cycle (θ) as function of the compressor offset. (b) Piston and (c) journal bearings friction power losses (P_{fr}) and maximum dimensionless eccentricities (ε_{max}) as function of the compressor offset (o_{cs}).

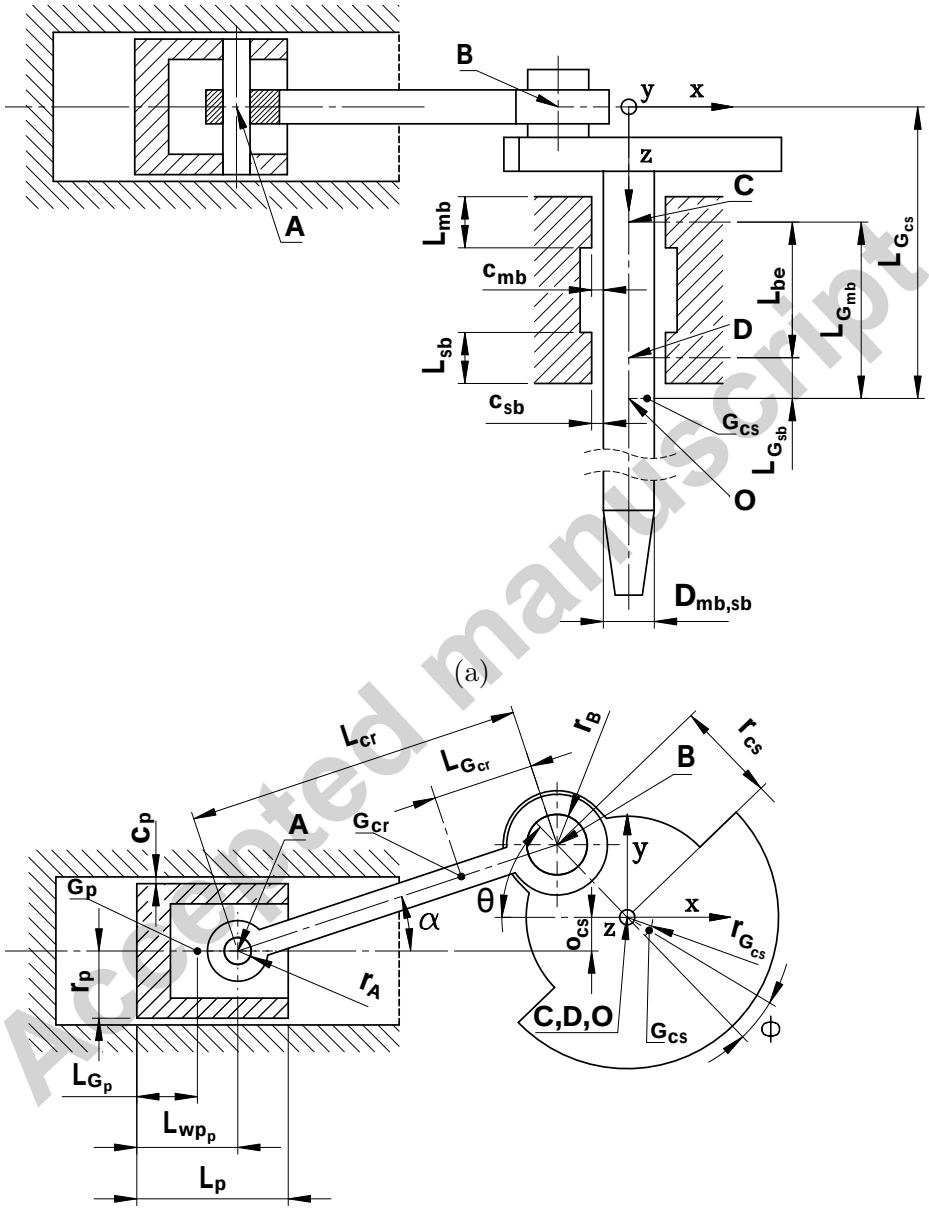

Figure 1: (a) Front view and (b) top view of the reciprocating compressor and its geometry.

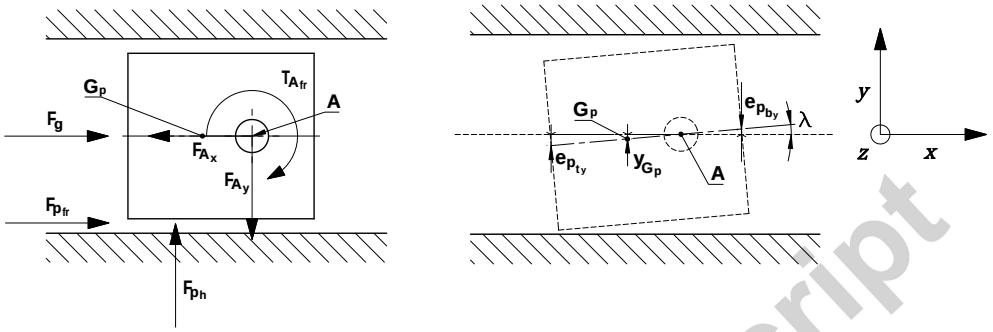

(a) (b)

Figure 2: Piston dynamic: (a) free body diagram and (b) a detailed image of its secondary movement.

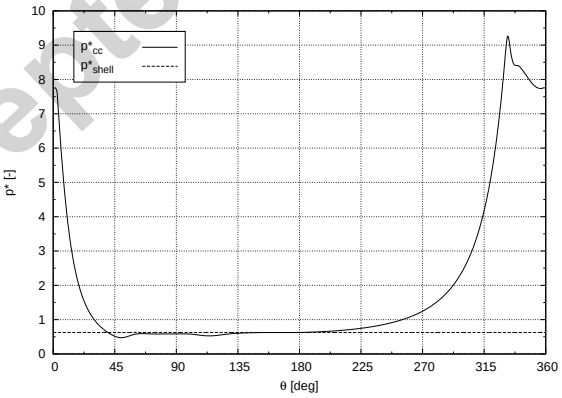

Figure 3: Dimensionless pressure in the compression chamber (p^*_{cc}) and the shell (p^*_{shell}) along the crank angle (θ).

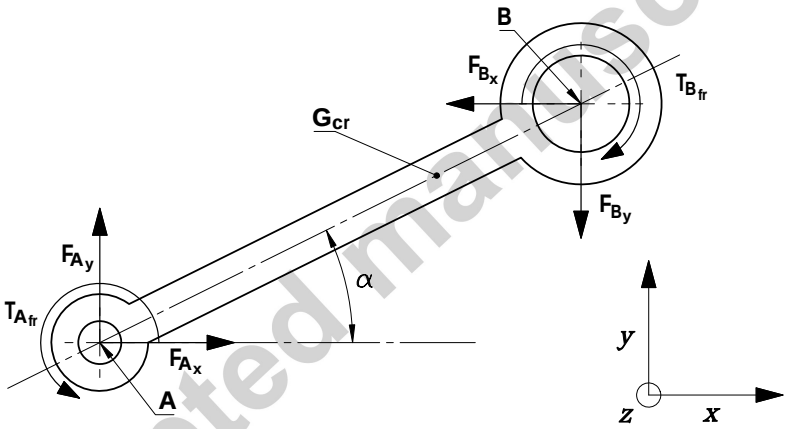

Figure 4: Connecting-Rod free body diagram.

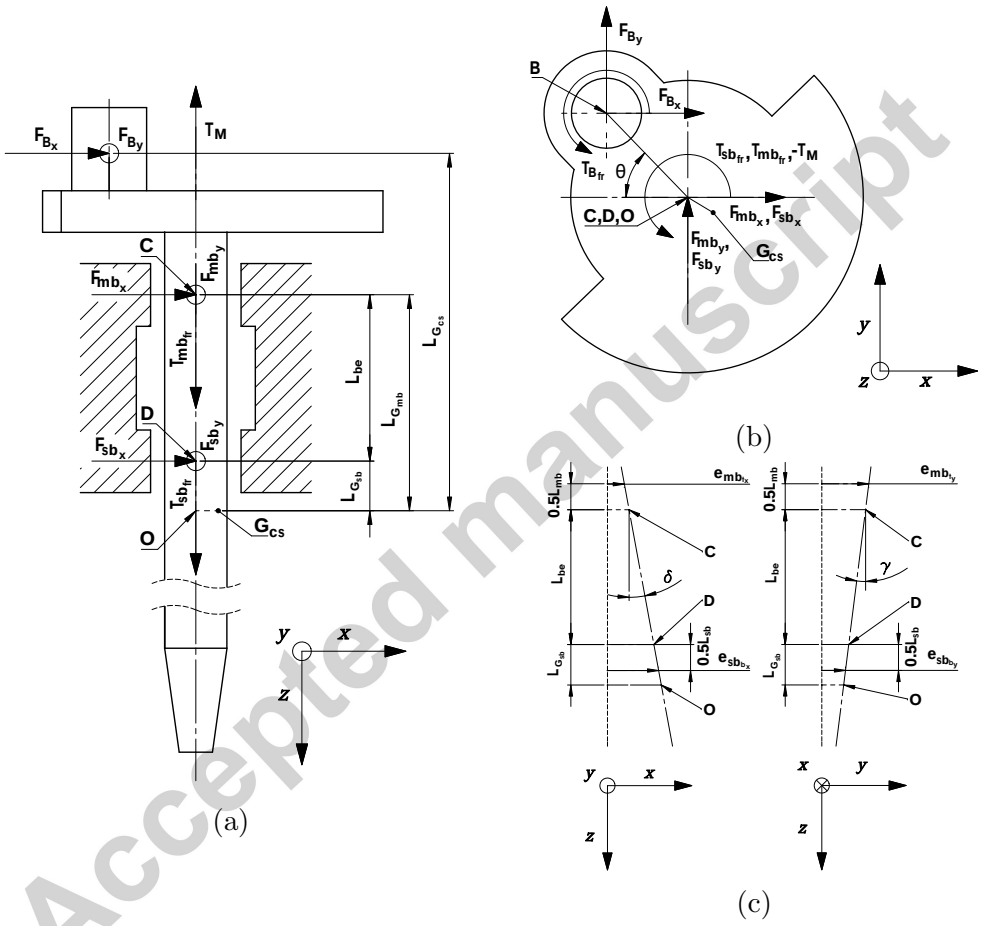

Figure 5: Crankshaft dynamics: (a) front and (b) top views of the free body diagram and (c) a detailed figure of its secondary movement, where the tilt line represents the crankshaft gyration axis.

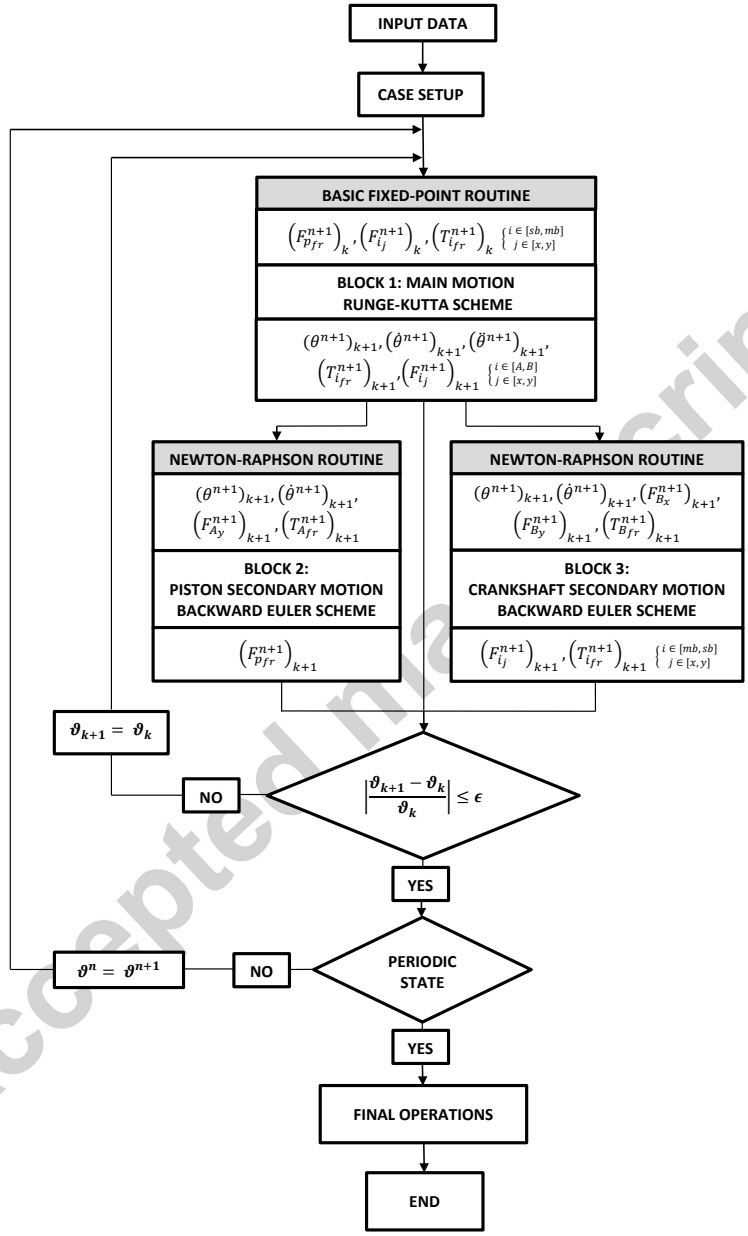

Figure 6: Global algorithm. The procedure is divided into three sub-iterative blocks. For simplicity, the ϑ symbol represents every unknown in the list. To assure a good coupling, the three blocks are resolved iteratively until convergence criterion (ϵ) is reached. The time advancing loop is repeated until each unknown achieves periodic state conditions.

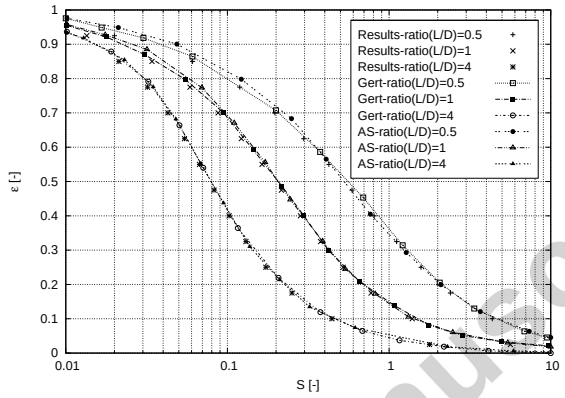

(a)

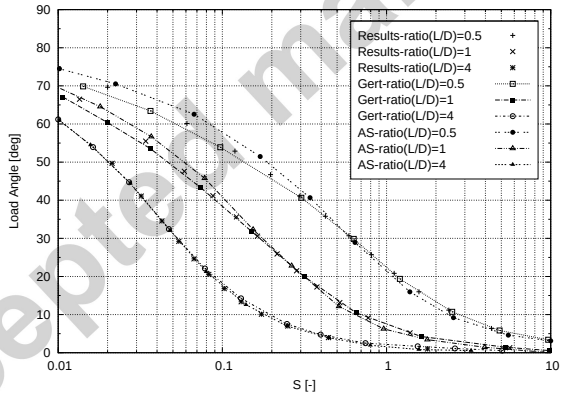

(b)

Figure 7: (a) Eccentricity and (b) load angle as function of the Sommerfeld number (S) of static and aligned journal bearing with different ratios L/D. Comparison between the code results (Results), the Gertzos' results [5] (Gert) and the results obtained by the analytical solution (AS) by Sfyris, D. and Chasalevris, A. [21]- [22].

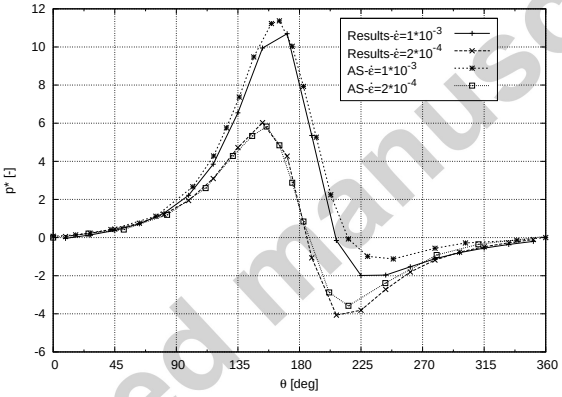

Figure 8: Dimensionless pressure distribution (p^*) along the angular coordinate θ in the axial centre of the bearing ($z = 0.5L_{mb}$) for different rates of change ($\dot{\varepsilon}$) and an eccentricity equal to 0.7. Comparison between the code results (Results) and the results obtained by the analytical solution (AS) by Sfyris, D. and Chasalevris, A. [21; 22].

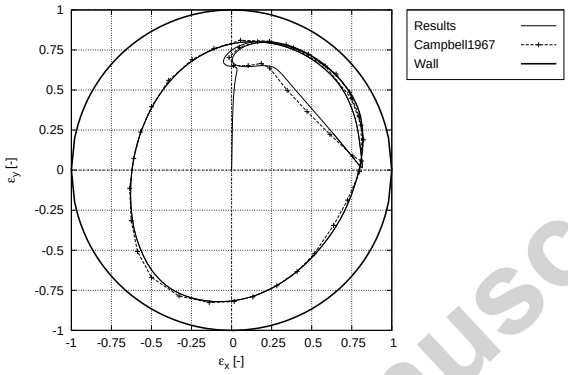

(a)

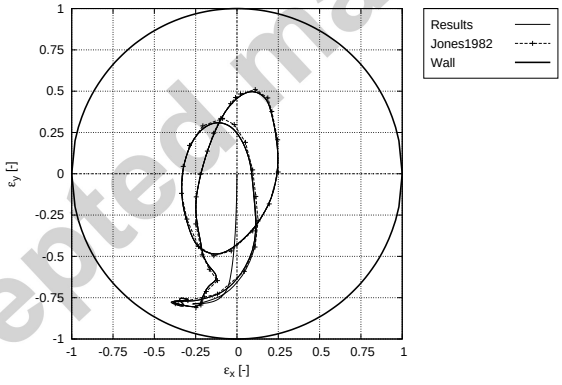

(b)

Figure 9: Trajectory of an aligned journal bearing under a dynamic load. Comparison between the code results (Results), and the (a) experimental results obtained by Campbell [1] and (b) the numerical results obtained by Jones [3].

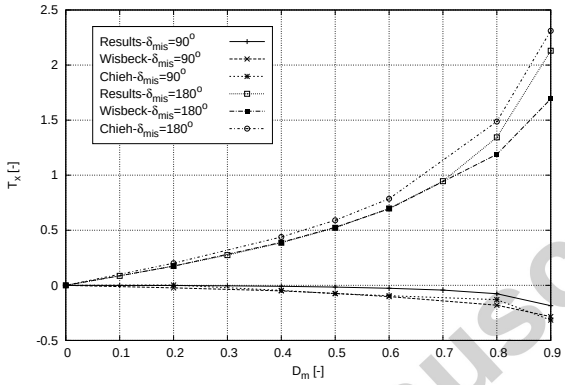

(a)

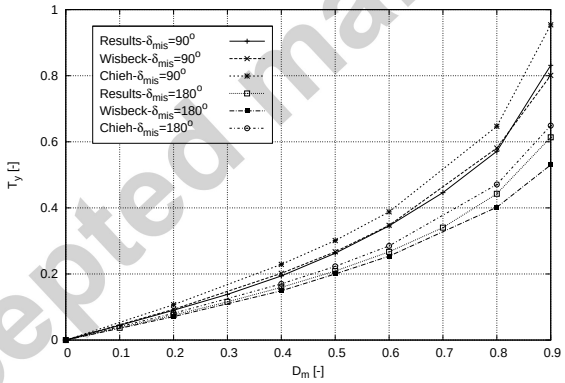

(b)

Figure 10: Dimensionless misalignment torques in the (a) x-direction a (T_x) and (b) y-direction T_y) as function of the misalignment degree (D_m) using different orientations (δ_{mis}). Comparison between the results obtained by Wisbeck, H.J. [23], and Chieh, H.[19] and the results obtained by the code.

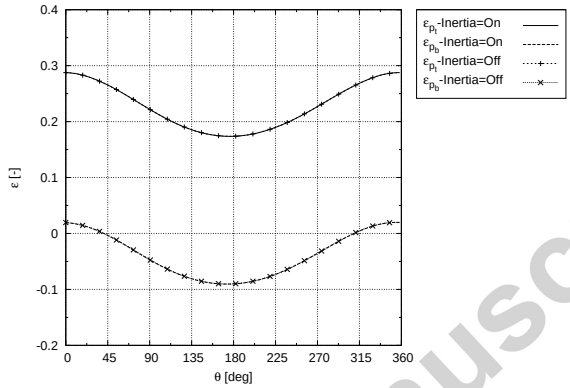

(a)

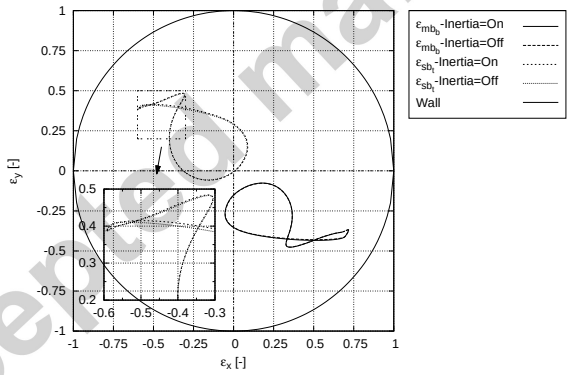

(b)

Figure 11: Comparison of the (a) piston and (b) crankshaft trajectories during a compressor cycle when the inertial forces in the secondary motion directions are considered and when they are not. The detailed view shows the differences among the secondary bearing trajectories.

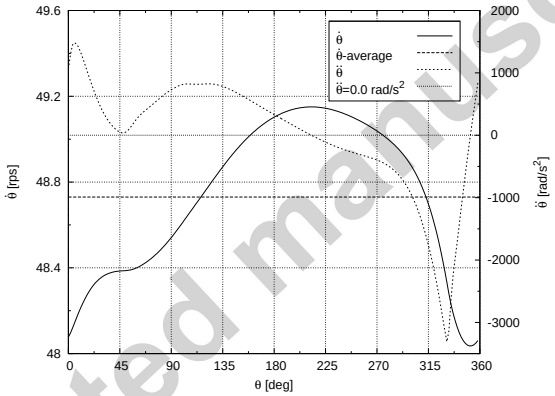

Figure 12: Crankshaft angular velocity ($\dot{\theta}$) and acceleration ($\ddot{\theta}$) along the compressor cycle (θ).

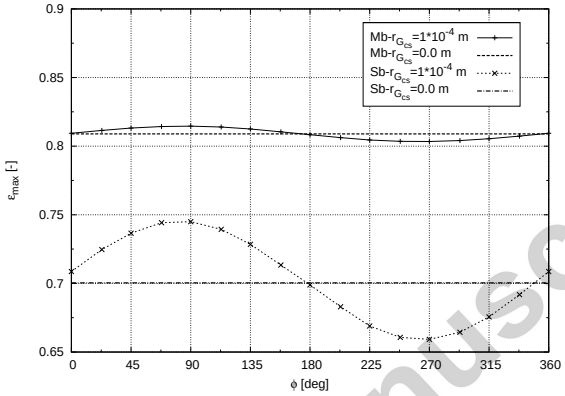

(a)

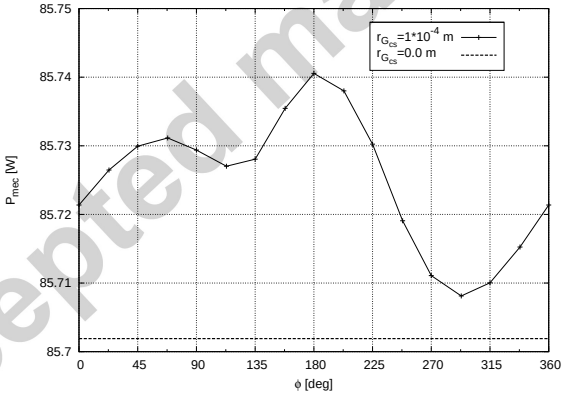

(b)

Figure 13: (a) Maximum dimensionless eccentricity (ε_{max}) of the main and secondary bearings and (b) compressor power consumption (P_{mec}) as function of the angular position of the crankshaft mass eccentricity (ϕ).

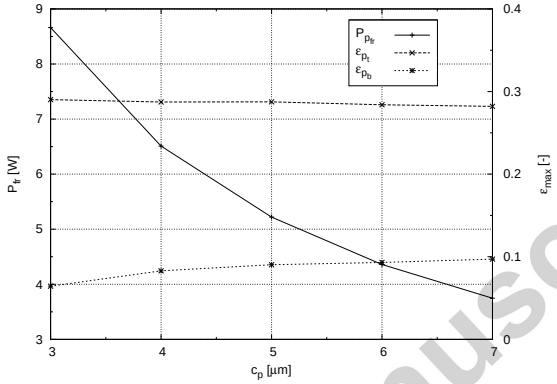

(a)

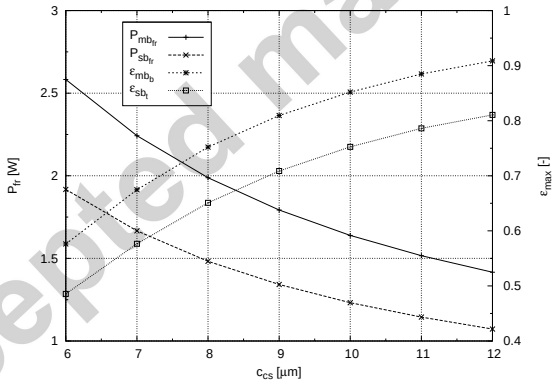

(b)

Figure 14: Friction power losses (P_{fr}) and maximum dimensionless eccentricities (ε_{max}) of (a) the piston as function of its clearance (c_p) and (b) the journal bearings as function of their clearances (c_{cs}).

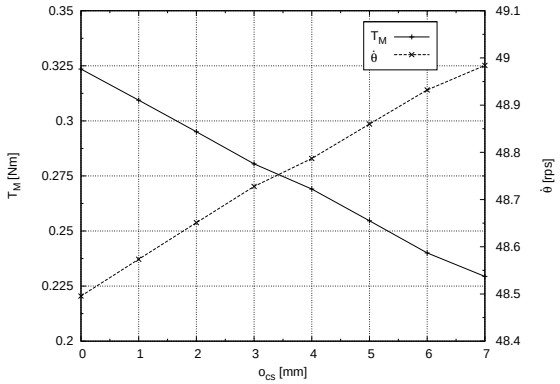

(a)

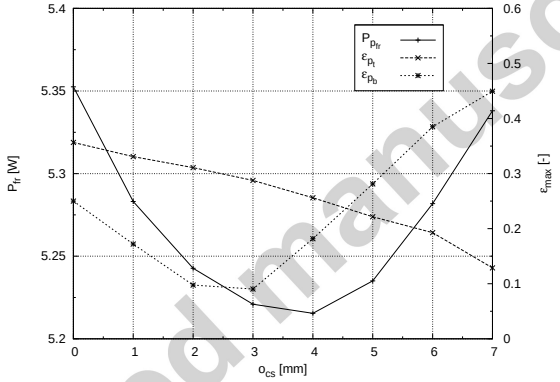

(b)

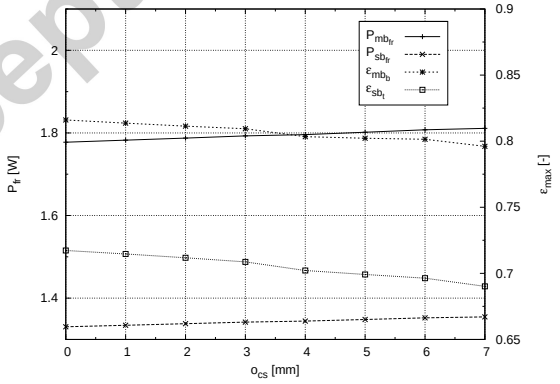

(c)

Figure 15: (a) Average motor torque (T_m) and average angular velocity ($\dot{\theta}$) during a compressor cycle (θ) as function of the compressor offset. (b) Piston and (c) journal bearings friction power losses (P_{fr}) and maximum dimensionless eccentricities (ε_{max}) as function of the compressor offset (o_{cs}).